

# Supramolecular Hydrogen Bond Enables Kapton Nanofibers to Reinforce Liquid-Crystalline Polymers for Light-Fueled Flight

Tianfu Song<sup>a,b</sup>, Huanyu Lei<sup>c</sup>, Adam J. Clancy<sup>d</sup>, Shudeng Ma<sup>a</sup>, Haifeng Yu<sup>a,\*</sup> and Liqun Zhang<sup>b,\*</sup>

<sup>a</sup> School of Materials Science and Engineering, and Key Laboratory of Polymer Chemistry and Physics of Ministry of Education, Peking University, Beijing 100871, China

<sup>b</sup> State Key Laboratory of Organic-Inorganic Composites, Beijing University of Chemical Technology, Beijing 100029, China

<sup>c</sup> South China Advanced Institute for Soft Matter Science and Technology, School of Molecular Science and Engineering, South China University of Technology, Guangzhou, 510641, China

<sup>d</sup> Department of Chemistry, University College London, 20 Gordon St., London WC1H 0AJ, UK

\*Corresponding author. E-mail: [yuhaifeng@pku.edu.cn](mailto:yuhaifeng@pku.edu.cn); [zhanglq@mail.buct.edu.cn](mailto:zhanglq@mail.buct.edu.cn)

## Abstract

We report fabrication of photoresponsive liquid-crystalline polymers reinforced with highly-oriented Kapton nanofibers with a supramolecular hydrogen bonding interface. To enhance the interfacial strength, hydroxyl groups are introduced into the side chain of azobenzene-containing liquid-crystalline polymers, forming hydrogen bonds with the Kapton nanofibers, directly imaged by nano-FTIR. Interestingly, the composite film exhibits the hierarchical structure of dragonfly wings, while demonstrating relatively high elastic modulus (1.64 GPa), reduced modulus (72.8 GPa), and nanohardness (4.5 GPa); 20 – 30 times higher than natural dragonfly wings. The enhanced mechanical performance and bilayer structure enables the composite film to exhibit rapid photoresponsive behaviors independent of the direction of illumination, due to an unconventional deformation mechanism arising from the interactions at the fiber-polymer interface. In addition, the flapping frequency and bending angle of the composite films can be continuously tuned for a single device (0.1 – 5 Hz, and 1.5 – 15.8°) by modifying the pulsed photoirradiation. The composite films are assembled into an artificial dragonfly device, and the light-driven flight aerodynamics are demonstrated in windy conditions. These not only provide a solution of micro-aircraft wings, but also offer a good bionic model for emulating dragonfly wings.

**Keywords:** Photomechanical composite, Liquid-crystalline polymer, Photoactuator, Micro aerial vehicle.

## 1. Introduction

Soft actuators transform molecular changes under external stimuli into macroscopic deformations leading to mechanical motion of devices. Their flexibility and potential have led to significant attention from researchers in a wide range of areas including chemistry, physics, robotics and engineering.<sup>[1-5]</sup> Liquid-crystalline polymers (LCPs) are among the most intensively studied, combining the anisotropy of LC ordering and the elastic deformation of polymers.<sup>[6-9]</sup> Notably, when azobenzene (AZ) chromophores are introduced as mesogens in LCP systems, light-driven soft actuators are readily obtained, enabling the actuator to be controlled using light as a non-contacted remote power source with high spatio-temporal resolution.<sup>[10-14]</sup> These AZ-containing LCPs convert light energy into photomechanical deformation, which has been used to power a wide array of motions to date including volume contraction/expansion, bending/unbending, folding/unfolding, twisting/coiling, and jumping.<sup>[15-22]</sup> The wide range of potential motions has led to a similarly wide range of biomimetic applications including self-regulating irises, worm-like crawling, predation of flytraps, swimming, etc.<sup>[23-28]</sup> However, while flapping has been obtained using an LCP network upon irradiation of high-intensity laser,<sup>[29]</sup> light-fueled flying devices are rare, due to the poor mechanical performance of AZ-containing LCPs.

The miniaturization of aircrafts involves volume/weight challenges,<sup>[30]</sup> particularly regarding engine and power source (e.g. fuel, batteries).<sup>[31]</sup> The use of a photo-driving method offers a route to circumnavigate these constraints, facilitating greatly reduced aircraft size and weight. A light-powered soft actuator based on LCP materials, designed to mimic the motion of insect wing oscillation, provides an ideal system for micro-aerial vehicle aviation. However, such a device requires sufficiently rapid response and actuation time, coupled to high mechanical performance of the airfoils, while maintaining a low total weight.<sup>[10,32-36]</sup> To satisfy these requirements for advancing micro-aircraft, two methods have been explored. First is to synthesize LCPs with ultrahigh molecular weight, which involves challenging synthesis and high-cost catalysts.<sup>[37]</sup> Second is to utilize polymer process engineering (e.g. compositing or blending with high performance polymers), which can be incorporated into classic LCPs as functional additives. Accordingly, carbon nanotubes (CNTs) have been used to reinforce LCPs, providing the composites with electrical conductivity and high elastic modulus.<sup>[19,20]</sup> However, both the high optical absorbance of CNTs and their intrinsic photothermal effect influences its light-responsive performance, and control over the CNT-LCP interface is challenging.

Here, to enhance the interfacial strength between LCPs and a mechanically-enhancing filler (Kapton nanofibers), we introduce hydroxyl groups into the side chain of photoresponsive LCPs, creating a supramolecular hydrogen bonding network with the reinforcement elements. The use of Kapton nanofibers provides high intrinsic mechanical performance as well as avoiding the absorbance/photothermal effects of carbon nanomaterial composite fillers. Interestingly, the fabricated LCP/Kapton nanofiber composite films exhibit analogical structures of natural dragonfly's wings, enabling them to be used as biomimetic model, promising for light-fueled micro-aircraft.

## 2. Material and Methods

### 2.1 Materials

The synthesis of the copolymer PM6AZCN<sub>m</sub>-r-PA4OH<sub>n</sub> (Figure S1a), calculation of the m:n ratio through <sup>1</sup>H-NMR (Figure S1b), and molecular weight characterization from gel-permeation chromatography are provided in the Supplementary Information (SI). The polyimide (Kapton) was synthesized according to a reported procedure.<sup>[42]</sup>

## 2.2 Preparation of nanofibers

The nanofiber film performed through typical electrospinning of 20 wt.% polyamide acid Kapton precursor DMF solution, using a spinning voltage of 20 kV, with a 210 μm diameter spinneret (27G gauge) and a 20 cm diameter rotating aluminum foil substrate. The speed of roller was set to 1500 rpm (from optimization trials to maximize fiber mat alignment) and a spinning time of 50 min was used to control the thickness of the fibrous film. These films were dried at 300 °C for 3 h for complete imidization of the polyamide acid. The volume fraction of nanofiber was 25 % - 40 %.

## 2.3 Preparation of the composite film

Composite films were prepared through fiber-composite lamination. Firstly, PM6AZCN<sub>2</sub>-r-PA4OH<sub>1</sub> (14 – 20 mg) was melted (130 °C, 20 min) onto glass coated with a sacrificial layer of sodium polystyrene sulfonate. Clean quartz was placed on the melt with two 25 × 5 × 0.025 mm spacers. The system was compressed using (2 kg weight, 30 min) to mitigate melt elasticity of the PM6AZCN<sub>2</sub>-r-PA4OH<sub>1</sub>. The melt was subsequently cooled on an iron plate and immersing in n-hexane. The n-hexane was evaporated under ambient conditions and a 25 × 20 × 0.015 mm nano-fibrous Kapton film (on an aluminum foil backing support) was placed on the film and pressure was applied, moving along the fiber orientation axis to maximize fiber/film contact. The system was compressed (2 kg) and then annealed (130 °C for 2 h, followed by 75 °C for 12 h). The crosslinking of the composite film was completed by a soaking method reported previously.<sup>[25]</sup> In short, the composite film was crosslinked in an adipoyl chloride/n-hexane solution (2 wt.%) for 3 days with one end clamped with a foldback clip. Finally, the crosslinked composite film was washed with n-hexane for 3 times and immersed in water for 20 min to remove the residual adipoyl chloride.

## 2.4 Molecular weight determination

Gel Permeation Chromatography (Waters 1515 Isocratic HPLC Pump) was performed on a tetrahydrofuran solution of P6AZCN<sub>2</sub>-r-P4OH<sub>1</sub> (8 mg/ml). The solution was placed in the dark for 24 h and filtered by a filter membrane immediately prior to testing.

## 2.5 UV-Vis absorption spectroscopy

The UV-Vis spectroscopy (Perkin Elmer, Lambda 750) of PM6AZCN<sub>2-r</sub>-PA4OH<sub>1</sub> was performed on a 0.1 mg/ml THF solution (SI, Figure S2a), and the photoisomerization of the PM6AZCN<sub>2-r</sub>-PA4OH<sub>1</sub> in the film status was shown in Figure S2c,d.

## 2.6 FTIR spectroscopy and Nano-IR spectroscopy

The temperature-dependent Fourier-transform infrared spectra (FTIR) was tested by Bruker Tensor II with the heating stage. The Nano-IR was characterized by Bruker nano IR2-FS and the scanning speed of mapping mode was 1.5 h per image.

## 2.7 Differential scanning calorimeter (DSC)

The thermodynamic property of PM6AZCN<sub>2-r</sub>-PA4OH<sub>1</sub> was characterized by two heating and cooling cycle by Mettler Toledo DSC1 with a heating/cooling rate of 10 °C / min. The two heating segments were both shown in Figure S2b.

## 2.8 Microstructure characterization

Polarized optical microscopy was performed on a Zeiss Scope A1. The micromorphology of nanofibrous film and the cross-section of composite film was characterized by scanning electron microscope (Hitachi S-4800).

## 2.9 Wide-angle X-ray scattering

Wide-angle X-ray scattering was performed on a Xenocs Xeuss 2.0 equipped with an *in\_situ* heating stage and a removable acceptor. Measurements were recorded between 2θ 2.5 – 25° for 4 h using a Cu Kα source (0.154 nm) at 50 kV with a sample distance of 376 mm. Heating and cooling was performed at a rate of 10 °C/min in vacuum and the parallel/perpendicular orientation was calibrated by scales on the heating stage.

# 3. Results and Discussion

## 3.1. Fabrication of the Composite Film

The LCP copolymer was synthesized through radical polymerization of a mixture of AZ-containing monomer 6-(4-(4'-cyanophenylazo)phenoxy)hexyl methacrylate (M6AZCN) and 4-hydroxybutyl acrylate (A4OH) at predetermined m:n molar ratio to give [PM6AZCN]<sub>m-r</sub>-PA4O<sub>n</sub> (Figure 1). Full synthetic details and polymer characterization are provided in the Supporting Information (SI). The AZ-containing PM6AZCN provides the photo-actuating characteristics and LC properties, while PA4OH was introduced to provide hydrogen bonding to the Kapton fiber surface to create a supramolecular interface with the nanofiber framework. The monomer stoichiometric ratio was selected as 2:1 to provide a balance between photoactuation and interfacial bonding, while minimizing the glass transition temperature (Figure S2b) to facilitate melt-infiltration of the PM6AZCN<sub>m-r</sub>-PA4OH<sub>n</sub> LCP into the nanofiber mat.

### (Figure 1)

Aligned Kapton nanofibers were used as a framework to enhance the mechanical performance of the AZ-containing LCP. Kapton (a polyimide consisting of 4,4'-oxydiphenylene-pyromellitimide units) is a commercially available and easily processable material, which can be spun into highly-aligned nanofibers through electrospinning. Mats of these aligned nanofibers have been used previously as an alignment layer for subsequent mesogenic materials, such as LC displays. Alignment was provided by electrospinning on a rotating drum; the alignment was quantified using the Hermann orientation factor ( $f = \frac{3\langle \cos^2\theta \rangle - 1}{2}$ ), reaching 0.85 after optimization through tuning the drum rotation speed. The average radius of the nanofibers was 300 – 500 nm and the surface of fibers was smooth (Figure S3).

### 3.2. Hierarchical Structure of the Composite Film

Composite films were assembled as a bilayer structure to improve the photoresponse cycle by accelerating the elastic recovery after photomechanical deformation, as has been undertaken previously for other soft photoactuators.<sup>[22,26]</sup> During the infiltration, the nanofibrous film thickness (10 – 15  $\mu\text{m}$ ) was set to half to the total LCP film thickness (25 – 30  $\mu\text{m}$ ), intrinsically forming the desired bilayer superstructure. The cross-section of the composite film was characterized with field emission scanning electron microscope (FESEM, Figure 2a); while a distinct boundary between two layers is not present, the LCP morphology is clearly modified on either half and fractured nanofibers are present only on one half of the composite. The structure of the resultant composite film demonstrated ordering across several length scales, from molecular-scale LCPs, to nanoscale Kapton fibers, and micrometer scale “nodes” (Figure 2c) formed from the overlapping Kapton fibers arising from the non-parallel nature of their aligned structure.

### (Figure 2)

In nature, dragonfly wings are 5 – 10 cm in length and 10 – 20  $\mu\text{m}$  in thickness, consisting predominantly of a thin protein membrane, supported by a network of stiff, hollow veins. As shown in Figure 2b, the vein structure isolates regions of membrane which varies in shape and size across the wing, with additional regions of reinforcement at the leading edge to further stabilize the wing. The veins themselves vary in size, stiffness, and contain micrometer vein nodes at the vein-membrane interface,<sup>[38,39]</sup> to provide a hierarchical structure to increase stiffness and disperse stress and pressure during flight.<sup>[40]</sup> As shown in Figure 2b, the obtained composite film exhibited analogous networks of “thread veins” (albeit less ordered than the naturally developed system), corrugations, and nodes, structural mimicking the surface morphology of dragonfly’s wings. Combined with the strong interface developed between the integrated materials (*vide infra*), this composite materials system has the attributes required for a promising bionic model of dragonfly wings.

### 3.3 Enhancement of Mechanics via Hydrogen Bond

In a similar manner to dragonfly wings, the hierarchical microstructure arising from the Kapton nanofibers mechanically reinforced the system, increasing the Young’s modulus along the orientation of fibers (1.637 GPa, Figure S4b, black line) from the pristine LCP film (0.441 GPa); the modulus orthogonal to the fiber direction has a significantly milder increase (0.452 GPa). The decrease in ultimate tensile strength (14.0 MPa parallel to the fibers versus 15.0 MPa for pristine LCP) is attributed to the wrinkled structures of composite film introducing local defects and initiating premature failure, and is more

significant orthogonal to the fiber direction (7.5 MPa) attributed to poorer shear transfer to the Kapton. The overall mechanical properties, particularly reduced modulus (72.8 GPa) and nanohardness (4.5 GPa) of these composite films are actually ca. 25 times higher than that of typical dragonfly (*Pantala flavescens*) wings.<sup>[40]</sup> The effective mechanical reinforcement is attributed to a strong interface between the LCP and the Kapton nanofibers, arising from hydrogen bonding interaction between polyimidic C=O and –OH on the PA4OH sidechains with the Kapton surface.<sup>[41]</sup> Temperature-dependent FTIR in the hydrogen bonding region (3650 – 3250 cm<sup>-1</sup>) demonstrate three characteristic peaks which sharpen upon heating, indicating three chemically distinct hydrogen bonding environments (Figure S5).

### (Figure 3)

Taking advantage of the similarities in microstructure between the produced LCP composite films and natural dragonfly wings, as well as the enhanced mechanical properties, artificial dragonfly-inspired micro-aircrafts wings were produced. The electrospinning and casting processing conditions are intrinsically adaptable,<sup>[42]</sup> allowing the morphology of nanofibers and LCP composites to be readily adjusted to simulate the shape of dragonfly wings (SI, Figure S9). This approach has the potential for the design of alternative novel wing structures by varying the distribution of nanofibers in the future, providing a model system to adapt for flexible and controllable micro-aerial vehicles.

### 3.4. Photomechanical Deformation of the Composite Film

Dragonfly flight involves continuous flapping of a pair of curved wings with varying speed to control motion.<sup>[38-40]</sup> A light-fueled biomimetic therefore requires both stable photomechanical deformation under irradiation, and the ability to tune oscillation frequency. Here, the oscillation is provided by combining a pulsed light power source with the fast response/recovery properties of the composite film. The pristine LCP film (fabricated by a general surface orientation method, without Kapton nanofibers) bends away from the light source under illumination, attributed to the "light-induced expansion" effect.<sup>[27,28]</sup> In contrast, the composite film showed different photomechanical deformation behavior, always bending towards the bilayer side containing nanofibers,<sup>[22,26]</sup> independent of the incident light direction (Movie S1). Due to the reinforced mechanical properties from the hydrogen bonded-Kapton fibers, this motion was capable of lifting a load 40× the mass of the film itself (Movie S2).

At room-temperature, neither the **pristine film nor the composite film** showed any significant mesogenic alignment under polarizing optical microscopy (POM, Figure S6), however, when the composite film was heated to the LC regime ( $\geq 90$  °C), the POM displayed clear birefringence (Figure S7). Due to highly thermal stability of the Kapton nanofibers, the mesoscale structure was clearly visible, even after the birefringence disappeared by heating the sample above the clearing point. This behavior was also observed in crosslinked composite films (Movie S3), which shows spontaneous reorientation. Notably, the composite film under irradiation only bent perpendicular to the orientation of nanofibers which couldn't be simply explained by classic "molecule synergistic motion" theory.<sup>[12,43-44]</sup>

To study the unusual photomechanical behaviors, WAXS was measured with *in situ* heating to monitor the LC domain ordering both parallel (Para) and perpendicular (Perp) to the nanofibers, at different temperatures. The WAXS measurement temperatures were determined by DSC across two heating cycles

(Figure S8a), selecting either side of significant features. The disparity between heating cycles is ascribed to a melting of the crystallization region in the first heating cycle, common for semi-crystalline polymers. The WAXS at room temperature (Figure S8b,c) shows a diffuse peak at  $20^\circ$ , typical of nematic LC phases, with a smaller, broad peak centered at  $7.5^\circ$  corresponding to the length of trans-AZ units (1.26 nm, Figure 4a). During the heating-cooling cycling, the intensity of the AZ-peak behaved anisotropically, with a lower signal perpendicular to the nanofibers than parallel to the nanofibers (Figure 4a). The WAXS indicates an alignment change of AZ mesogenic units (Figure 4b), under heating and, therefore, under irradiation, although further work is needed to fully characterize this reorientation behavior. Further analysis is complicated, however, by scattering effects limiting *in situ* optical characterization (e.g., UV-Vis spectroscopy) due to the scattering effects of nanofibers and the thick films.

#### (Figure 4)

Combining the POM and WAXS with the observed LCP properties, we propose a mechanism for the unusual photomechanical deformation of the aligned composite films. UV illumination is known to both increase the free volume in AZ-containing LCPs and decrease their glass transition temperature.<sup>[45,46]</sup> For the composite film here, most of the AZ moieties maintain trans-isomers during the illumination because the composite film is thicker than 1  $\mu\text{m}$ . We note that thicker films have even poorer light penetration, and a greater fraction of material remains in the trans-isomer, and total bending of the film decreases. In addition, the UV-Vis spectra indicate only 80% cyano-AZ isomerized in solution after 1 s irradiation of UV light (100  $\text{mW}/\text{cm}^2$ , Figure S2c); it is likely that a lower degree of isomerization occurs in solid composite film. The free volume of the LCP increases when composite films are illuminated/heated and the nanofibers will hinder local motion, however, the main LCP chain does not strongly inhibit local motion of the AZ units due to the presence of relatively flexible PA4OH spacers. As a result, under illumination, the AZ mesogens can align along the long axis of nanofibers by capillary force, shrinking perpendicular to the fibers. Once illumination ceases and/or the composite is cooled, the free volume decreases leading the polymer layer to elastically ‘spring back’ creating a uniaxial tensile force perpendicular to the fibers. The bilayer nature of the composite is key to accelerating this elastic recovery of the photomechanical deformation, in addition to providing the incident light direction-independent actuating behavior. The rapid recovery is accentuated by the selection of cyano-AZ in the synthesized LCPs which inherently possesses fast back-isomerization versus other AZ components,<sup>[12,43-44]</sup> allowing the trans-cis-trans cycle to run continuously.

### 3.5 Photoactuating Behaviors of the Composite Film

To create functional micro-aircraft from the LCP composite, its photomechanical motion must be controlled, requiring an understanding of the relationships between bending angle/vibration frequency, and the intensity/pulse rate of the powering light source. As shown in Figure 5a, the composite film vibration under pulsed light demonstrated a continuum of tunable behaviors as a function of intensity and the frequency of the light. The photoinduced motion of composite films under 460 nm light is similar to 365 nm irradiation,<sup>[54]</sup> so the latter was used for mapping parameter space as it simultaneously allows simpler photography of the moving device. Photomechanical bending angles at 0.1 Hz exhibit a decreasing slope with increasing light intensity, likely related to the gradient of the light intensity penetrating through the

composite film thickness. When the light intensity is fixed, faster pulse frequencies lead to photoinduced bending angles decreasing, following an exponential decay (confidence coefficient > 0.99, Figure 5a). Upon photoirradiation with the 5.0 Hz pulse light (the highest frequency tested), the photomechanical bending angles of all intensities decreased to a very low level (ca. 1.5°). The attenuation of vibration angles at fixed light intensity is attributed to the high viscosity of the polymer at room temperature. While cyano-AZ reorientation is thought to be intrinsically capable of 5 Hz cycling, the polymer backbone is hydrogen-bonded to the nanofibers, so could not follow the fast switching of the uniaxial force field, decelerating the excluded free volume/reorientation process. As a result, the vibration angle of the composite film decays to a minimum value. The full parameter space may be mapped as an "actuation surface" (Figure 5b) illustrating the diverse range of photomechanical oscillation motions with vibration frequency, for micro-aircraft wings (Movie S4).

When it comes to the material choice of micro-aircraft, especially ornithopters, the ability to continuously manipulate the frequency and speed of the oscillation motion is key. These characteristics may be defined by the ratio of bending angle ( $A_{\text{bend}}$ ) to both actuating time ( $t_{\text{bend}}$ ) and recovery speed ( $t_{\text{recovery}}$ ). In contrast to previous actuators (including LCP networks,<sup>[21,28,47-49]</sup> photothermal materials,<sup>[50,51]</sup> solvent-responsive materials, and hydrogels<sup>[52]</sup>), the composite film here provides a continuum of oscillation behaviors, controllable with the incident light pulse frequency and intensity (Figure S11), covering a wide range of possible behaviors. Importantly, in contrast to previous work, the actuating behavior may be modified externally for a single device by changing the frequency and intensity of the powering light. Further, these properties have been obtained using intrinsically stable materials (particularly versus photothermal/solvent responsive materials) and are driven by low-power actuating light, ideal for micro-aircraft systems.

(Figure 5)

### 3.6. Light-Driven Motion of Artificial Dragonfly Wings

The actuating composite film wings were assembled into an artificial dragonfly device to study its aerodynamics during the light-fueled flight (Figure 6), creating a simple model system to demonstrate the potential of the composite film in a flying device. Natural dragonflies are complicated,<sup>[55,56]</sup> and the contributing components and mechanisms cannot be fully duplicated, but notably involve twin pairs of wings flapping in opposing directions for propulsion, and air sacs to provide buoyancy. Here, the latter was modelled using a helium balloon attached to the device with fishing line (2 m, Figure S9). The photo-inert components were made from glass capillaries, attached to two pairs of wings obtained from cutting composite films vertical to the orientation of nanofibers, as shown in Figure S9. The shape and size of wings correspond to those of a scaled-down real dragonfly, with a length of 2 cm; the weight fraction of the composite film in the device is 3.4%, slightly higher than that of real dragonflies.<sup>[40]</sup> Under the illumination, the forewings and the hindwings were respectively designed to bend upwards and downwards to simulate the phase difference during the flight of natural dragonfly. The balloon/artificial dragonfly assembly formed a pendulum system where the pendulum length is 200 times of the dragonfly length, making it very sensitive to minor changes, thus suitable for aerodynamic studies. By controlling the quantity of helium in the balloon, the artificial dragonfly could float in air and move freely.

### (Figure 6)

A breeze (3 – 5 m/s) was blown from a helium cylinder, which was precisely adjusted by a control valve. In the helium breeze, the artificial dragonfly swung in a 2.6 cm region due to the unstable airstream and cyclones between the wall and the artificial dragonfly. Blue light (460 nm) was chosen for photo-actuation, since the visible light is environmentally friendly in practical applications. Upon irradiation, the artificial dragonfly tended to "escape" from the light spot, diving ca. 1 – 3 cm, with a maximum displacement 6.5 cm from the initial position (Figure 6a, Movie S5). Interestingly, this kind of diving movement is common in the landing, hunting and oviposition of dragonflies.<sup>[53]</sup> In our preliminary model, the lift force produced by each composite film-wing "flap" is responsible for the diving motion of the artificial dragonfly. Elevation of the device from the flapping led to loss of tension in the line connecting the dragonfly to the balloon.

To monitor the aerodynamics of the diving motion, the artificial dragonfly was tracked under the 4.0 m/s gas flow, and the displacement of the device was recorded. Constant illumination was used in place of pulsed irradiation to simplify the system and limit turbulence from wing oscillations which would significantly complicate the analysis. Prior to illumination (but under gas flow), the maximum displacement of the artificial dragonfly was 2.6 cm from the initial position, however, upon irradiation, five dives could be seen over 30 s (Figure 6b, Figure S10). Further, each dive demonstrated three distinct phases, as seen from smaller displacement peaks either side of the primary peak (Figure 6b, inset). The first peak is from the first 'flap' causing a change in the distribution of airflows, producing a lift force larger than the gravitational force on the artificial dragonfly.<sup>[53]</sup> After the device was lifted towards the supporting balloon, the tension in the connecting wire was removed, reducing its contribution to the total upwards force. After the flapping ceased (by moving out of the illuminated region), the lift force also disappeared, and the artificial dragonfly descended under gravity, until the pendulum line was straightened again, restoring an upwards force through tension. However, the inertia from the fall led to a continued dive, which was eventually overcome by the tension in the pendulum wire, leading to an acceleration upwards and subsequent inertia in the upwards direction (of lesser magnitude than the preceding fall). The oscillation caused here is seen as the post-dive small peak, and in some cases a second set of oscillations was seen before the system returned to the initial position (Figure 6c).

## 4. Conclusion

We fabricated a photomechanical composite film by introducing highly oriented nanofibers into an AZ-containing LCP film to successfully improve mechanical performance. Interestingly, the structure of the composite film demonstrated order across several length scales, simulating a bio-inspired structural architecture of the natural dragonfly wings. The composite films undergo photomechanical bending independent of the direction of incident light, with fast recovery of the photoinduced deformation. The actuating mechanism is attributed to photoinduced volume expansion and mesogenic reorientation driven by capillary forces between the nanofibers. The actuation of the films shows a continuum of behaviors in terms of bending angle and frequency, with a single device's behavior tunable with the intensity and frequency of pulsed light. The ability to tune behavior using external stimuli on the same material/device distinguishes the created films here from previously developed photo-actuators, overcoming a key hurdle

towards light-powered micro-aircrafts. This composite system has extensive possible application in systems requiring externally tunable, mechanically reinforced photoactuator, including the micro-aircrafts demonstrated here, water-propulsion, remote robotics, haptic devices, flow controllers, and artificial muscles. To demonstrate the potential of this new system, a light-powered artificial dragonfly-mimetic device was created, constituting the first ever micro-aircrafts flown with the LCP/Kapton nanocomposites actuators. The aerodynamic behavior of the device in light-driven motion in air has been characterized and shows great promise as the foundation for the next generation of micro-aircraft.

## Funding

This work was sponsored by the financial support from the National Key R&D Program of China (2018YFB0703702, 2017YFB0306903), the National Natural Science Foundation of China (Grant No.s 51773002, 51921002, 51988102, 51790501, 51221002 and 51521062). AJC would like to thank The Society of Chemical Industry and the Ramsay Memorial Trust for funding.

## References

- [1] D. Dattler, G. Fuks, J. Heiser, E. Moulin, A. Perrot, X. Yao, N. Giuseppone, *Chem. Rev.* 2020,120, 310. doi:10.1021/acs.chemrev.9b00288
- [2] M. Sitti, D. S. Wiersma, *Adv. Mater.* 2020, 32. 1906766. doi:10.1002/adma.201906766
- [3] H. Bisoyi, Q. Li, *Chem. Rev.* 2016,116, 15089. doi:10.1021/acs.chemrev.6b00415
- [4] H. Zeng, P. Wasylczyk, D. S. Wiersma, and A. Priimagi, *Adv. Mater.* 2018, 30, 1703554. doi:10.1002/adma.201703554
- [5] F. Lancia, A. Ryabchun, N. Katsonis, *Nat. Rev. Chem.* 2019, 3, 536. doi:10.1038/s41570-019-0122-2.
- [6] H. Finkelmann, H. J. Kock, H. Rehage, *Makromol. Chem. Rapid Commun.* 1981, 2, 317. doi:10.1002/marc.1981.030020413
- [7] H. Finkelmann, E. Nishikawa, G. G. Pereira, M. Warner, *Phys. Rev. Lett.* 2001, 87, 15501. doi:10.1103/physrevlett.87.015501
- [8] T. Ikeda, J. Mamiya and Y. Yu, *Angew. Chem. Int. Ed.* 2007, 46, 506. doi: 10.1002/anie.200602372
- [9] M. Warner, E. M. Terentjev, *Prog. Polym. Sci.* 1996, 21, 853. doi: 10.1016/S0079-6700(96)00013-5
- [10]. Y. Yu, M. Nakano, T. Ikeda, *Nature* 2003, 425, 145. doi: 10.1038/425145a
- [11] D. C. Pilz, M., M. Debije, A. Schenning, *Chem. Soc. Rev.* 2020, 49, 6568. doi: 10.1039/D0CS00363H
- [12] H. Yu, T. Ikeda, *Adv. Mater.* 2011, 23, 2149. doi: 10.1002/adma.201100131
- [13] T. Seki, *Bull. Chem. Soc. Jpn.* 2018, 91, 1026. doi: 10.1246/bcsj.20180076
- [14] X. L. Pang, J. Lv, C. Y. Zhu, L. Qin, Y. L. Yu, *Adv. Mater.* 2019, 31, 1904224. doi: 10.1002/advs.202002464
- [15] M. Li, P. Keller, B. Li, X. Wang, M. Brunet, *Adv. Mater.* 2003, 15, 569 doi: 10.1002/adma.200304552

- [16] Z. Liu, ; R. Tang,; D. Xu, J. Liu, H. Yu, *Macromol. Rapid Commun.* 2015, 36, 1171. doi: 10.1002/marc.201500177
- [17] S. Iamsaard, S. J. Asshoff, B. Matt, T. Kudernac, J. J. L. M. Cornelissen, S. P. Fletcher, N. Katsonis, *Nature Chem.* 2014, 6, 229. doi: 10.1038/nchem.1859
- [18] M. Zmyślony, K. Dradrach, J. Haberko, P. Nałęcz-Jawecki, M. Rogóż, P. Wasylczyk, *Adv. Mater.* 2020, 32, 2002779. doi: 10.1002/adma.202002779
- [19]. X. Sun, W. Wang, L. Qiu, W. Guo, Y. Yu, H. Peng, *Angew. Chem. Int. Ed.* 2012, 51, 8520. doi: 10.1002/ange.201201975
- [20] W. Wang, X. Sun, W. Wu, H. Peng, Y. Yu, *Angew. Chem. Int. Ed.* 2012, 51, 4644. doi: 10.1002/ange.201200723
- [21] K. M. Lee, M. L. Smith, H. Koerner, N. Tabiryan, R. A. Vaia, T. J. Bunning, T. J. White, *Adv. Funct. Mater.* 2011, 21, 2913. doi: 10.1002/adfm.201100333
- [22] X. Lu, H. Zhang, G. Fei, B. Yu, X. Tong, H. Xia, Y. Zhao, *Adv. Mater.* 2018, 30, 1706597. doi: 10.1002/adma.201706597
- [23].R. Verpaalen, M. Pilz Da Cunha, T. A. P.Engels, M. G. Debije, A. P. H. J. Schenning, *Angew. Chem. Int. Ed.* 2020, 59, 4532 doi: 10.1002/anie.201915147
- [24] A. H. Gelebart, D. J. Mulder, M.l Varga, A. Konya, G. Vantomme, E. W. Meijer, Robin L. B. Selinger, D. J. Broer, *Nature* 2017, 546, 632 doi: 10.1038/nature22987
- [25] S. Ma, X. Li, S. Huang, J. Hu, H. Yu, *Angew. Chem., Int. Ed.* 2019, 58, 2655 doi: 10.1002/anie.201811808
- [26] H. Zeng, O. M. Wani, P. Wasylczyk, R. Kaczmarek, A. Priimagi, *Adv. Mater.* 2017, 29, 1701814. doi: 10.1002/adma.201701814
- [27] H. M. van der Kooij, S. A. Semerdzhiev, J. Buijs, D. J. Broer, D. Liu, J. Sprakel. *Nat. Comm.* 2019, 10, 3501 doi: 10.1038/s41467-019-11501-5
- [28] K. Kumar, C. Knie, D. Bléger, M. A. Peletier, H. Friedrich, S. Hecht, D. J. Broer, M. G. Debije, A. P. H. J. Schenning. *Nat. Comm.* 2016, 7, 11975. doi: 10.1038/ncomms11975
- [29].T. J. White, N. V. Tabiryan,S. V. Serak,U. A. Hrozhyk,V. P. Tondiglia, H. Koerner, R. A. Vaia, T. J. Bunning, *Soft Matter* 2008, 4, 1796. doi: 10.1039/B805434G
- [30].P. Lequeu, P. Lassince, T. Warner, G.M. Raynaud. *Aircr. Eng. Aerosp. Tec.* 2001, 73, 147. doi:10.1108/00022660110386663
- [31] I. Sher, D. Levinzon-Sher, E. Sher, *Appl. Therm. Eng.* 2009, 29, 400. doi: 10.1016/j.applthermaleng.2008.03.020
- [32]. I. Cabrera, V. Krongauz, H. Ringsdorf, *Angew. Chem., Int. Ed.* 1987, 26, 1178 doi: 10.1002/anie.198711781
- [33] S.H. Chen, H.M.P. Chen, Y. Geng, S.D. Jacobs, K.L. Marshall, T.N. Blanton, *Adv. Mater.* 2003, 15, 1061 doi: 10.1002/adma.200304836
- [34] K. F. Nelson, W. E. Haas, J. E. Adams, *J. Electrochem. Soc.* 1974, 121, 1667. doi: 10.1149/1.2401766
- [35] T. Ikeda, H. Shin, K. Durga B., K. Seiji, T. Shigeo, *Chem. Lett.* 1988, 17, 1679 doi: 10.1246/cl.1988.1679

- [36] R. Brettle, D. A. Dunmur, N. J. Hindley, C. M. Marson, *Chem. Commun.* 1992, 410. doi: 10.1039/C39920000410
- [37] J. Lv, Y. Liu, J. Wei, E. Chen, L. Qin, Y. Yu, *Nature* 2016, 537, 179. doi: 10.1038/nature19344
- [38] X. Wang, Y. Lin, Y. Shi, *Compos. Sci. Technol.* 2008, 68, 186. doi: 10.1016/j.compscitech.2007.05.023
- [39] A. Azadeh, D. Abolfazl, Y. T. Mehdi, *J. Bionic Eng.* 2018, 15, 859. doi: 10.1007/s42235-018-0073-1
- [40] Y. Zhao, D. Wang, J. Tong, J. Sun. *J. Bionic Eng.* 2016, 13, 388. doi: 10.1016/S1672-6529(16)60312-8
- [41] T. Steiner, *Angew. Chem. Int. Ed.* 2002, 41, 48; *Angew. Chem.* 2002, 144, 50. doi: 10.1002/1521-3773(20020104)41:1<48::AID-ANIE48>3.0.CO;2-U
- [42] H. Lei, J. Lu, G. Dong, G. Tian, S. Qi, D. Wu, *Dyes Pigm.* 2019, 161, 79. doi: 10.1016/j.dyepig.2018.09.036
- [43] A. Natansohn, P. Rochon, *Chem. Rev.* 2002, 102, 4139. doi: 10.1021/cr970155y
- [44] Z. Cheng, S. Ma, S. Huang, Y. Chen, Y. Zhang, H. Yu, *Macromolecules* 2017, 50, 8317. doi: 10.1021/acs.macromol.7b01741
- [45] H. Zhou, C. Xue, P. Weis, Y. Suzuki, S. Huang, K. Koynov, G. K. Auernhammer, R. Berger, H. Butt, S. Wu, *Nature Chem.* 2017, 9, 145. doi: 10.1038/nchem.2625
- [46] J. Algers, P. Sperr, W. Egger, L. Liszkay, G. Kögel, J. de Baerdemaeker, F. H. J. Maurer, *Macromolecules* 2004, 37, 8035. doi: 10.1021/ma0486086
- [47] M. Lahikainen, H. Zeng, A. Priimagi, *Nat. Comm.* 2018, 9, 4148 doi: 10.1038/s41467-018-06647-7
- [48] C. Li, J. Yun, H. Kim, M. Cho, *Macromolecules* 2016, 49, 6012 doi: 10.1021/acs.macromol.6b01002
- [49] B. Yang, F. Cai, S. Huang, H. Yu, *Angew. Chem., Int. Ed.* 2020, 59, 4035. doi: 10.1002/ange.201914201
- [50] L. Dong, X. Tong, H. Zhang, M. Chen, Y. Zhao, *Mater. Chem.* 2018, 2, 1383 doi: 10.1039/C8QM00190A
- [51] F. Ge, X. Lu, J. Xiang, X. Tong, Y. Zhao, *Adv. Mater.* 2015, 27, 7867. doi: 10.1002/adma.201502777
- [52].X. Peng, T. Liu, C. Jiao, Y. Wu, N. Chena, H. Wang, *J. Mater. Chem. B* 2017, 5, 7997. doi: 10.1039/C7TB02119D
- [53].Adrian L. R. Thomas, G. K. Taylor, R. B. Srygley, R. L. Nudds, R. J. Bomphrey, *J. Bionic Eng.* 2004, 207, 4299. doi: 10.1242/jeb.01262
- [54] P. Zhang, B.Wu, S. Huang, F. Cai, G. Wang, H. Yu, *Polymer*, 2019, 178, 121644.doi: 10.1016/j.polymer.2019.121644
- [55].Z. J. Wang, *Annu. Rev. Fluid Mech.* 2005. 37:183. doi: 10.1146/annurev.fluid.36.050802.121940
- [56].S. P. Sane, *The J. Exp. Bio.* 2003, 206, 4191. doi: 10.1242/jeb.00663

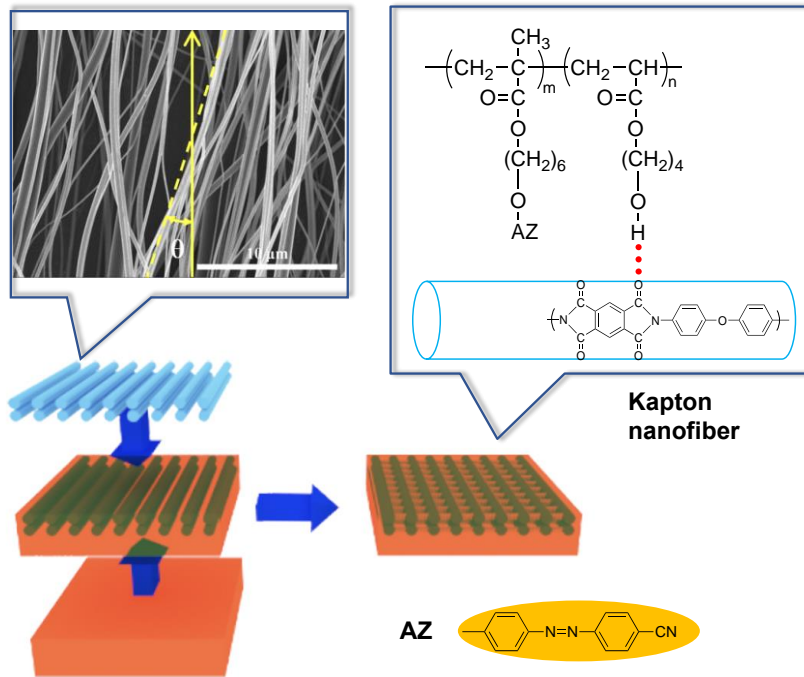


**Figure 1.** Preparation of the composite film of highly-oriented Kapton nanofiber-reinforced AZ-containing LCPs, with interfacial hydrogen bonding (red dashed line).

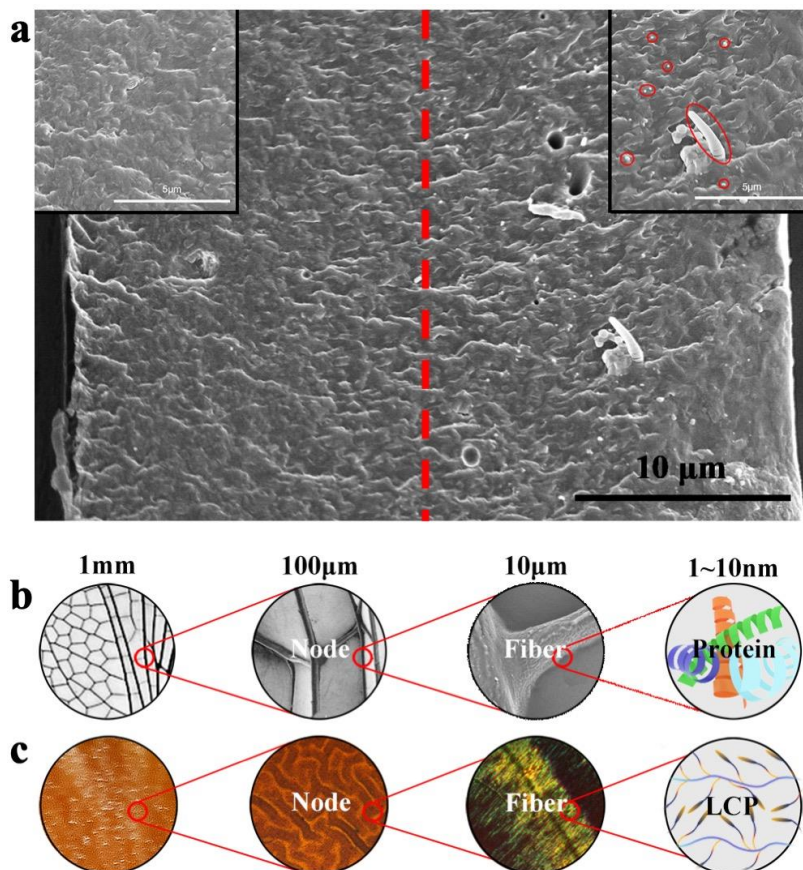


**Figure 2.** The structure of the composite films. (a) SEM micrograph of film cross-section showing the bilayer structure of the composite film; inserts highlight fiber-containing (top right) and fiber-free (top left) regions. (b,c) The analogous hierarchical structures of (b) natural dragonfly wing and (c) the composite film.

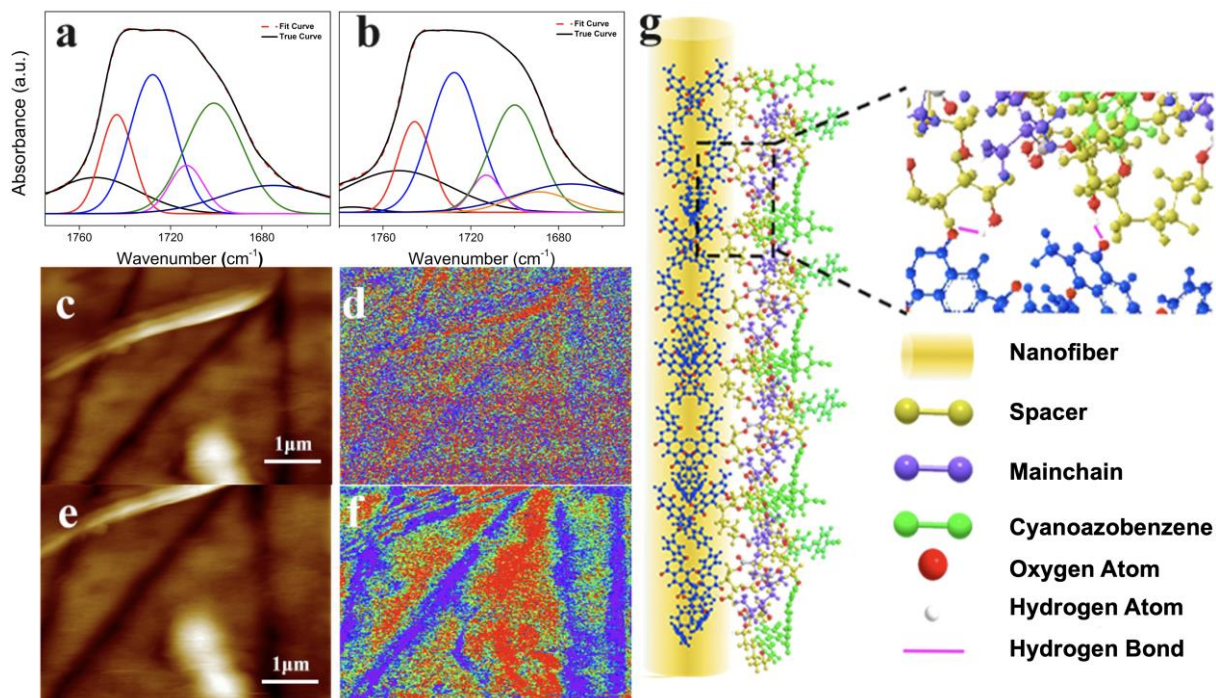


**Figure 3.** Hydrogen bonding distribution in the composite films. (a,b) Peak-fitted FTIR spectra of (a) pristine film and (b) composite film. (c-f) Nano-IR mapping of composite film with AFM height profiles (c,e, z-scale range 0 – 200 nm) and respective FTIR intensity maps (d,f) at separate wavelengths: (d)  $1688\text{cm}^{-1}$  (orange line in b), (f)  $1724\text{cm}^{-1}$  (blue line in a,b). Normalized intensities provided on low-high/blue-red scale. (g) Proposed structure of interface in the composite film, from Nano-FTIR mapping.

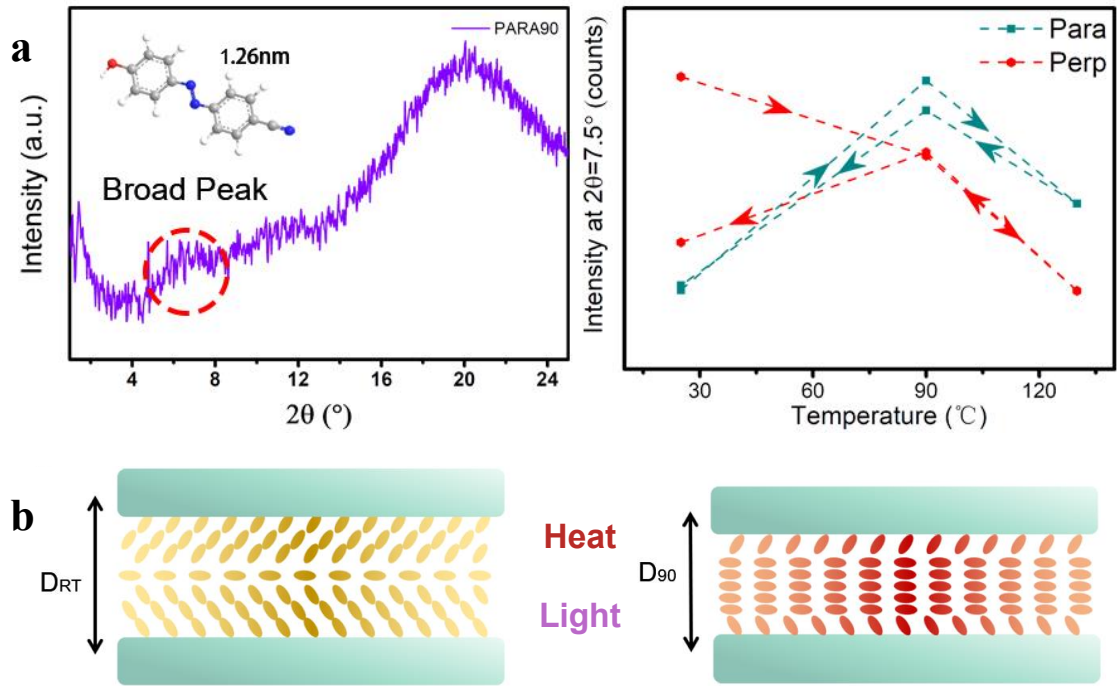


**Figure 4.** Deformation mechanism of composite film under illumination/heating (a) WAXS diffractogram of composite films (left) at  $90^{\circ}\text{C}$  during the cooling segment, highlighting the broad peak at  $2\theta = 7.5^{\circ}$ , and (Right) intensity of the broad peak at  $2\theta = 7.5^{\circ}$  during temperature cycling. (b) Schematic of proposed mechanism of the photoresponsive behavior of the composite film (note  $D_{RT} > D_{90}$ ).

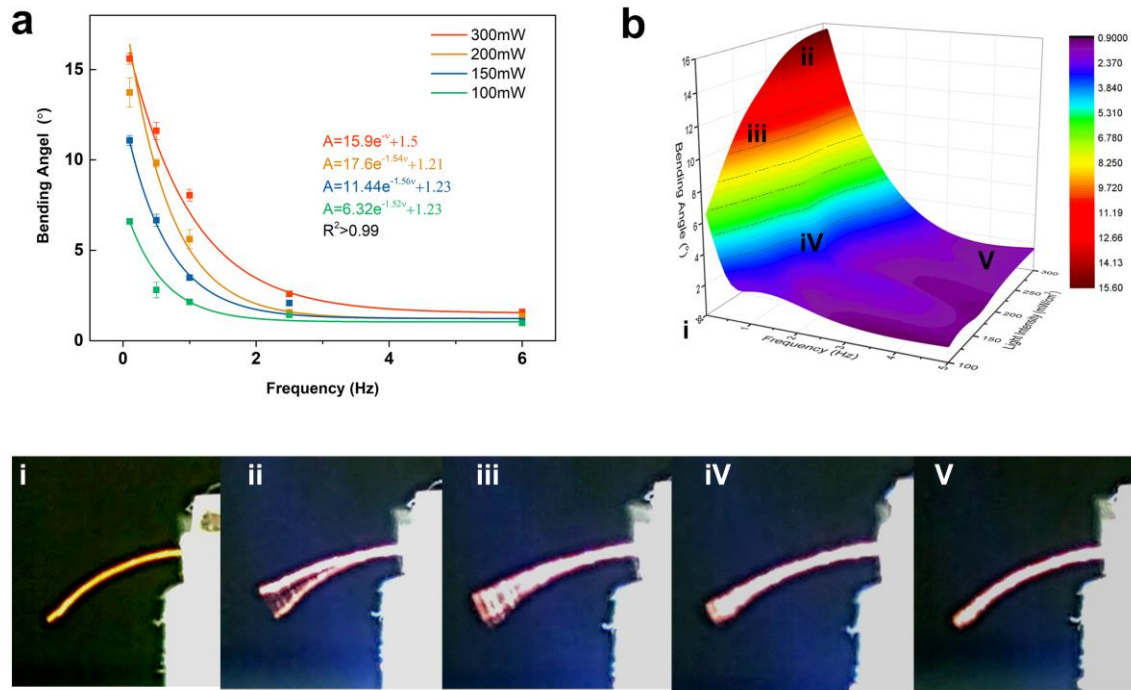


**Figure 5.** The flapping properties of composite films. (a) The bending angles of composite films with different light intensities and pulse frequencies; (b) The 3D mapping plot of the “actuating surface” of pulse frequency (x-axis), light intensity (y-axis), and bending angle (z-axis), with time-lapse photos (i-v) of composite films illuminated by different 365 nm pulse LED light with 10 s exposure time, with corresponding conditions highlighted on the actuating surface plot: (i) Film under no illumination with intrinsic bending attributed to the different moduli of within the bilayer structure; (ii)(v) Composite films in the gliding region with a low flapping frequency and large bending angle; (iii)(iv) Pictures of composite films in the flapping region with a high flapping frequency and small bending angle. The boundary is determined by  $\partial A / \partial v =$  variance of data per group where we regard the vibration of composite films as “flapping”.

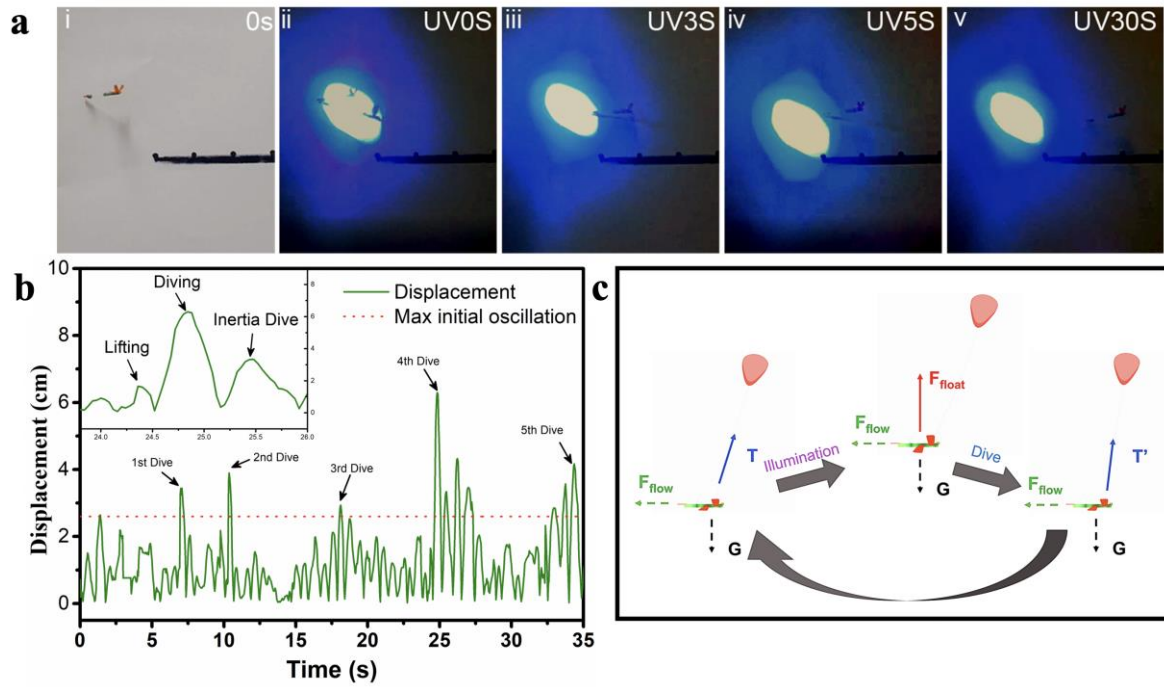


**Figure 6.** The design and the light-driven motion of the artificial dragonfly device. (a) Digital photographs of device diving motion under blue light 0, 3, 5, and 30 s after illumination. (b) Track chasing curve of artificial dragonfly device and the displacement-time curve. (c) The principle scheme of the light-driven dive.